Overcoming Anomalous Suppression of M-Plane AlGaN Growth by Molecular-Beam Epitaxy Using Indium as a Surfactant

Brandon Dzuba<sup>1,2</sup>, Trang Nguyen<sup>1</sup>, Yang Cao<sup>1</sup>, Rosa E. Diaz<sup>2</sup>, Michael J. Manfra<sup>1,2,3,4</sup>, Oana Malis<sup>1,2\*</sup>

<sup>1</sup>Department of Physics and Astronomy, Purdue University, West Lafayette, Indiana 47907, USA

<sup>2</sup>Birck Nanotechnology Center, West Lafayette, Indiana 47907, USA

<sup>3</sup>School of Electrical and Computer Engineering, Purdue University, West Lafayette, Indiana 47907, USA

<sup>4</sup>School of Materials Engineering, Purdue University, West Lafayette, Indiana 47907, USA

An anomalous growth rate reduction and associated composition divergence with increasing aluminum flux in m-plane AlGaN grown by plasma-assisted molecular beam epitaxy (PAMBE) at low temperature (565°C) is observed and investigated. We find that the AlGaN growth rate under conventional gallium-rich conditions decreases rapidly with increasing aluminum flux, contrary to expectations. Moreover, the aluminum fraction of these layers increases super-linearly with aluminum flux, indicating substantial nitrogen and gallium loss from the crystal surface. Indium surfactant assisted epitaxy (ISAE) is found to mitigate this effect significantly. ISAE AlGaN layers do not exhibit a significant decrease in growth rate with increasing aluminum flux, and their aluminum compositions increase linearly with aluminum flux. Transmission electron microscopy (TEM) images reveal the presence of high aluminum composition defects within the conventionally grown AlGaN layers, which are significantly reduced in ISAE AlGaN layers. Spatial correlation of these defects with local areas of reduced growth rate observed in an (In)Al<sub>0.30</sub>Ga<sub>0.70</sub>N/In<sub>0.16</sub>Ga<sub>0.84</sub>N multiple quantum well (MQW) structure suggests that these

<sup>\*</sup> Author to whom correspondence should be addressed. Electronic mail: <a href="mailto:omalis@purdue.edu">omalis@purdue.edu</a>

phenomena have a causal relationship. We attribute the growth rate reduction to loss of nitrogen and gallium due to site blocking effects of aluminum adatoms. TEM imaging indicates that high-quality, virtually defect-free (In)Al<sub>0.24</sub>Ga<sub>0.76</sub>N/In<sub>0.16</sub>Ga<sub>0.84</sub>N MQWs can be grown at 565°C with negligible indium incorporation into the barriers.

#### 1. Introduction

The III-nitride material system has long been a promising candidate for the development of a variety of devices, such as high-electron-mobility transistors, light-emitting diodes, laser diodes, and other novel optoelectronic devices. 1 This is primarily due to their large bandgap, which ranges from 0.64 eV in InN<sup>2</sup> to 6.2 eV in AlN.<sup>3</sup> In particular, nitride multi-quantum well (MQW) structures are of interest for near-infrared (NIR) optoelectronic devices due to their large conduction band offsets (CBO). However, MQW devices using the conventional (0001)-oriented GaN substrates are hindered by strong built-in spontaneous and piezoelectric polarization fields.<sup>4,5</sup> The natural solution to this issue is to eliminate built-in polarization fields by designing the structures on nonpolar substrate orientations, such as the  $(10\overline{1}0)$ -oriented m-plane. The second major challenge of nitride MQW is the significant lattice mismatch between different III-nitride alloys that results in high degrees of strain accumulation. Strain leads to defect formation and ultimately cracking with detrimental effects on device performance.<sup>6</sup> Therefore, strain-balancing has been proposed as a technique to mitigate strain accumulation in heterostructures using oppositely strained layers.<sup>7</sup> On GaN substrates, this is achieved by alternating tensile-strained AlGaN layers with compressively-strained InGaN layers. This paper presents a study of the structure of PAMBE grown m-plane AlGaN and strain-balanced InGaN/AlGaN MQWs for NIR intersubband (ISB) optoelectronic devices.

M-plane  $(10\overline{1}0)$ -oriented AlGaN/InGaN MQWs are ideal candidates for near-infrared (NIR) ISB devices. These structures are free from the effects of internal polarization fields, 8-10 have

built-in strain mitigation, and can achieve CBOs large enough for NIR transitions when sufficiently large aluminum and indium compositions are used. Recently, we reported PAMBE of high-quality m-plane InGaN with up to 0.16 indium metal fraction, 11 but this requires growth at low temperature. near 565°C. AlGaN growth by conventional gallium-rich methods at this temperature is compromised by low adatom diffusion lengths and the inability to desorb gallium, resulting in inhomogeneous material and asymmetric AlGaN/InGaN structures, respectively. 12 We have shown that ISAE eliminates these issues in low aluminum content m-plane AlGaN, while also significantly improving surface roughness, interface quality, and photoluminescence (PL) of MQW structures. 12 Studies conducted via metal organic chemical vapor deposition (MOCVD) on a variety of surface orientations have also shown ISAE reduces defects<sup>13,14</sup> in AlGaN layers while producing atomically flat surfaces. 15 Monroy et al. 16 and Pramanik et al. 17 experimentally showed the surfactant effects of indium during the growth of c-plane AlGaN layers by PAMBE, and this effect has been theoretically described by Neugebauer et al. 18 However, we also found unintentional indium incorporation in m-plane AlGaN grown by ISAE [referred to as (In)AlGaN] at low temperature. This reduces the bandgap of the material and shifts the lattice constant closer to GaN, resulting in a CBO below that required for NIR devices while also significantly reducing the strain balancing effect.<sup>12</sup> Therefore, it is necessary to investigate the growth of low temperature m-plane (In)AlGaN by PAMBE to minimize this undesirable indium incorporation and ensure ISAE AlGaN can be used as a strain balancing layer in various devices.

In this work, we report the results of a detailed study of a series of low temperature m-plane gallium-rich AlGaN layers and ISAE (In)AlGaN layers across a wide range of aluminum fluxes on m-plane GaN. Shirazi et al. previously observed a significantly reduced growth rate in high-composition m-plane  $Al_yGa_{1-y}N$  layers (y > 0.50) grown at high temperature (720°C). However, this has not yet been confirmed at low aluminum composition or low temperature.

We find that as the Al flux increases, the growth rate of gallium-rich AlGaN layers decreases super-linearly, despite nitrogen limited growth conditions. Moreover, the Al composition also

increases super-linearly with Al flux, suggesting that gallium and nitrogen are prevented from incorporating into the lattice. Interestingly, application of an indium surfactant restores the expected AlGaN epitaxy. The growth rate of (In)AlGaN bulk samples is not significantly affected by Al flux, and composition increases linearly with increasing Al flux. High-resolution scanning transmission electron microscopy (HR-STEM) images of a 30 repeat (In)Al<sub>0.30</sub>Ga<sub>0.70</sub>N/In<sub>0.16</sub>Ga<sub>0.84</sub>N MQW structure reveal that the reduction in growth rate is linked to the formation of high-Al containing defects within the material. Understanding and controlling these processes allowed us to grow low temperature (In)AlGaN layers with negligible indium incorporation, resulting in the demonstration of a 15 repeat strain-balanced (In)Al<sub>0.24</sub>Ga<sub>0.76</sub>N/In<sub>0.16</sub>Ga<sub>0.84</sub>N MQW structure with a CBO theoretically suitable for NIR optical transitions.

## 2. Experimental

All films were grown by PAMBE on commercially available m-plane  $(10\overline{1}0)$  free-standing GaN substrates with a -0.5° ± 0.2° miscut toward the (0001) direction purchased from Nanowin Science and Technologies. The substrates have a threading dislocation density <  $5x10^6$  cm<sup>-2</sup> and a root mean square (RMS) roughness of < 0.3 nm over a  $4x4~\mu m^2$  area. The substrates were sonicated in trichloroethylene (TCE), acetone, and methanol, rinsed with deionized water, and then dried with N<sub>2</sub> gas. Before entering the PAMBE chamber, the substrates were outgassed overnight (> 12 hours) at ~500°C in an ultra-high vacuum (UHV) chamber attached to the PAMBE. The substrates were then loaded into a PAMBE system equipped with conventional effusion cells for aluminum, indium, gallium, and silicon. A Veeco Unibulb radio-frequency (RF) plasma source is used to supply atomic nitrogen to the chamber. Prior to the active layer, an ~150 nm GaN buffer layer is grown at 720°C under gallium-rich conditions. This results in a GaN surface with pronounced step-terraces and RMS < 0.3 nm, as measured by atomic force microscopy (AFM) on control samples.

Metal fluxes were measured with a beam flux gauge and recorded as beam equivalent pressure in units of torr. These measurements were converted to flux estimates in units of atoms/cm²s using known material densities and calibration samples of In<sub>0.09</sub>Ga<sub>0.91</sub>N, Al<sub>0.20</sub>Ga<sub>0.80</sub>N, and InN for gallium, aluminum, and indium, respectively. All samples reported here were grown with a N<sub>2</sub> flow rate of 0.5 sccm and a RF power of 300W. Thickness measurements made from transmission electron microscopy images of GaN grown under nitrogen-limited conditions suggest these nitrogen parameters correspond to a ~7.9 nm/min GaN growth rate, yielding ~5.8x10<sup>14</sup> atoms/cm²s active nitrogen flux.

X-ray diffraction (XRD) measurements were made with a Panalytical MRD X'Pert Pro High-Resolution diffractometer. Modeling of XRD  $\omega$ -20 scans was done with the software package Epitaxy 4.5a provided by Malvern PANalytical and was used to determine the thickness and composition of all bulk films. These models assume uniform material, and the growth rates and compositions extracted from them represent an average throughout the material. Vegard's law was used to calculate the lattice parameters of ternary alloys. Using the density of GaN, each growth rate was converted to an effective nitrogen flux ( $\Phi_N^{eff}$ ) in atoms/cm²s, representing the approximate number of nitrogen adatoms incorporated into the lattice per unit area per unit time. Since the aluminum sticking coefficient at these temperatures is unity, for (In)AlGaN layers we assumed all provided aluminum adatoms are incorporated into the structure. Individual layer growth rates and compositions in MQW structures cannot be determined directly through XRD  $\omega$ -20 scans. Therefore, to model these structures the material growth rates and compositions are assumed to be similar to those in AlGaN and InGaN bulk layers grown under similar conditions.

All samples in this study were grown at 565°C under metal rich conditions, such that nitrogen was the limiting component. This low growth temperature was chosen to achieve sufficient indium incorporation in (In)AlGaN/In<sub>0.16</sub>Ga<sub>0.84</sub>N MQW for NIR applications.<sup>12</sup> A series of m-plane AlGaN bulk films of increasing aluminum flux was grown to study their structure and morphology. Three

of those samples were grown gallium rich. This was verified experimentally by either the observation of metallic droplets on their surface or by observation of a significant reflection high energy electron diffraction (RHEED) intensity recovery time upon termination of metal flux under constant nitrogen flux. Three additional films were grown with an indium surfactant using the same aluminum flux as the gallium-rich samples. The gallium flux of these samples was set such that  $\Phi_{Al} + \Phi_{Ga} \ge \Phi_N^{eff}$ , thus resulting in layers with little to no indium incorporation. One monolayer of indium was pre-deposited prior to (In)AlGaN growth. An indium flux of approximately 0.93x10<sup>14</sup> atoms/cm²s was used for the (In)AlGaN sample with the highest aluminum flux. All other (In)AlGaN samples were provided a decreased indium flux of 0.57x10<sup>14</sup> atoms/cm²s to reduce droplet formation without sacrificing surfactant capabilities. The growth time for all bulk films was 345 seconds.

Indium incorporation in the (In)AlGaN layers was evaluated by modeling XRD  $\omega$ -2 $\theta$  scans under the assumption that the AlN growth rate is identical to the growth rate derived from XRD for the gallium-rich AlGaN layer grown with the same Al flux. Note that for the sample grown with the largest Al flux (1.72x10<sup>14</sup> atoms/cm<sup>2</sup>s), this method was not possible due to inhomogeneity of the gallium-rich layer. Therefore, this AlN growth rate was estimated by assuming it scales linearly with beam equivalent pressure. Simulations of XRD  $\omega$ -2 $\theta$  scans for the bulk (In)AlGaN layers using the above assumptions revealed peak positions that closely matched the experimental spectra. We take this as an indicator that little to no indium incorporated into these layers, as any significant indium incorporation would shift the measured peak position to lower angles.

(In)AlGaN/InGaN MQW structures were also grown under conditions similar to the bulk samples, but with  $\Phi_{Al} + \Phi_{Ga} \approx \Phi_N^{eff}$ . The InGaN layers in the MQWs were grown with excess indium as described previously. Since indium incorporation at 565°C is limited by thermal decomposition, the InGaN growth rate and composition were assumed to be the same as those of a thick In<sub>0.16</sub>Ga<sub>0.84</sub>N layer grown under the same conditions. Indium was provided to the barriers

of these structures using a modulated deposition scheme similar to that used in our previous work<sup>12</sup> to minimize droplet formation. In contrast to our previous work,<sup>12</sup> additional gallium flux was provided during (In)AlGaN barrier growth to compensate for the increased growth rate observed in the presence of indium surfactant. The Indium flux is similar to that used in Ref. 12. Consequently, the net III/N ratio in this work is increased relative to our previous work. Note that in our previous work<sup>12</sup>  $\Phi_{Al} + \Phi_{Ga} < \Phi_N^{eff}$  due to our lack of understanding of the change in growth rate in the presence of indium surfactant. Most important, XRD analysis similar to that described for (In)AlGaN layers indicated that these adjusted fluxes resulted in negligible indium incorporation in the barriers. We believe this is because gallium and aluminum incorporate before indium and use up all available nitrogen adatoms. This method also prevented excess gallium from incorporating into the InGaN layers.

The bulk and MQW m-plane structures were investigated with high-angle annular dark-field scanning transmission electron microscopy (HAADF-STEM). HAADF-STEM acquisition was done with a double aberration-corrected Thermo Scientific Themis Z TEM/STEM at 300kV acceleration voltage and 0.23nA current. Samples were prepared using the focused ion beam (FIB) *in situ* lift-out method on a Thermo Scientific Helios G4 UX Dual Beam. 500V polishing and plasma cleaning were conducted on the lamellas to reduce high-energy ion beam damage and contamination.

### 3. Results and Discussion

The average growth rate and composition for all measured m-plane AlGaN bulk films are summarized in Figure 1(a) and Figure 1(b), respectively. Under metal rich conditions, we expect the growth rate to be independent of metal flux. However, for gallium-rich grown structures, we find that the nitrogen limited growth rate decreases with increasing aluminum flux. This surprising decrease is super-linear with Al-flux, and at our highest measured aluminum flux results in a

sample with almost half the expected growth rate (Figure 1(a)). The gallium-rich samples also show a super-linear increase in aluminum content (Figure 1(b)), which follows from the decrease in incorporated nitrogen adatoms coupled with aluminum's preferential incorporation over gallium.<sup>20</sup> Note that the reported growth rate and composition for the gallium-rich film with the highest aluminum flux are rough estimations; this is due to inhomogeneous material, likely partial relaxation, and large variations in the sample thickness. Samples grown by ISAE, however, show a negligible decrease in growth rate with increasing aluminum flux (Figure 1(a)), and a linear increase in aluminum content (Figure 1(b)). This suggests that ISAE efficiently suppresses the anomalous decrease of m-plane AlGaN growth rate with increasing aluminum flux.

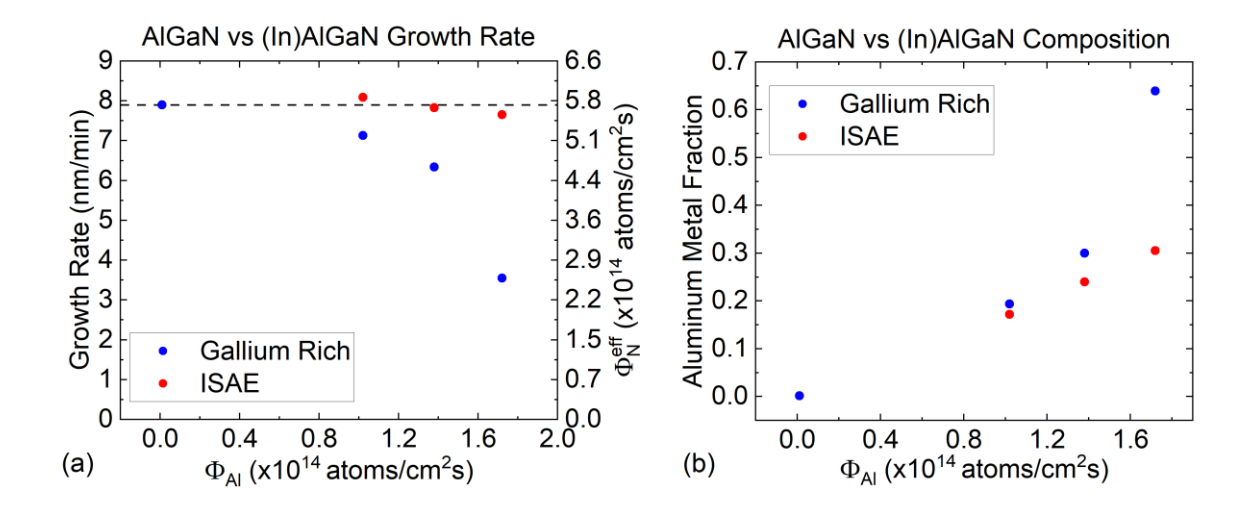


**Figure 1.** Plot of the growth rate (a) and aluminum metal fraction (b) of AlGaN (blue) and (In)AlGaN (red) layers grown under varying aluminum fluxes. The black dashed line represents the nominal m-plane GaN growth rate under gallium-rich conditions. AlGaN layers were grown under gallium-rich conditions, while (In)AlGaN were grown under an indium surfactant. All samples contain less than 0.01 mole fraction of indium as modeled by XRD.

HR-STEM images were taken of several samples to verify the film thicknesses as well as investigate their material quality (Figure 2). Figure 2(b) shows the (In)Al<sub>0.30</sub>Ga<sub>0.70</sub>N layer which was provided an aluminum flux of ~1.72x10<sup>14</sup> atoms/cm<sup>2</sup>s. To compare with this ISAE sample, HR-STEM images were taken of a gallium-rich structure with an identical aluminum composition (Figure 2(a)) and a gallium-rich structure grown with an identical aluminum flux (Figure 2(c)). The AlGaN samples are significantly thinner than the (In)AlGaN sample. The gallium-rich structure with identical aluminum composition to the ISAE sample was grown with a reduced aluminum flux of ~1.38x10<sup>14</sup> atoms/cm<sup>2</sup>s to compensate for the reduced growth rate. Meanwhile, the gallium-rich sample which was provided an identical aluminum flux to the ISAE sample resulted in an average ~0.65 aluminum fraction. Note that due to this film's large variation in aluminum fraction

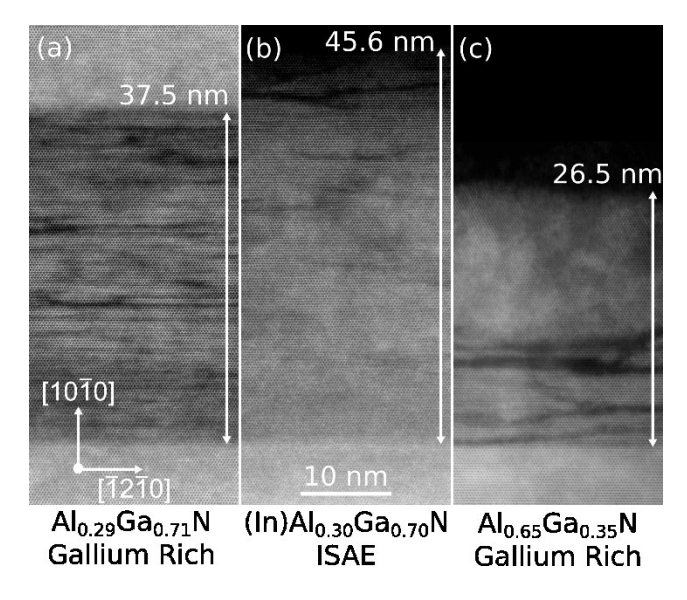


**Figure 2**. HR-STEM images of (a) a gallium-rich Al<sub>0.29</sub>Ga<sub>0.71</sub>N layer grown with  $\Phi_{Al} = 1.38 \times 10^{14}$  atoms/cm<sup>2</sup>s, (b) an (In)Al<sub>0.3</sub>Ga<sub>0.7</sub>N layer grown with  $\Phi_{Al} = 1.72 \times 10^{14}$  atoms/cm<sup>2</sup>s, and (c) a gallium-rich Al<sub>0.65</sub>Ga<sub>0.35</sub>N layer grown with  $\Phi_{Al} = 1.72 \times 10^{14}$  atoms/cm<sup>2</sup>s. Dark regions represent higher aluminum fraction due to the lower atomic mass of aluminum. A gallium cap layer is visible in (a), which was not grown for (b) or (c). The growth direction is along  $(10\overline{10})$ .

and thickness (11 nm - 29 nm as measured by large scale HR-STEM), this aluminum fraction is only a rough estimation based on the supplied aluminum flux and average film thickness.

HR-STEM of the ISAE structure (Figure 2(b)) shows a clear structural improvement when compared to the similar composition gallium-rich layer (Figure 2(a)). The (In)Al<sub>0.3</sub>Ga<sub>0.7</sub>N layer shows a significant reduction in the density of Al-rich areas, seen in HR-STEM as regions of darker contrast within the AlGaN layer, resulting in a more homogeneous material. This is similar to the improvement reported in our previous work for lower aluminum content MQW structures.<sup>12</sup> We note, however, that the indium surfactant is not sufficient to completely eliminate the high-aluminum defects from the (In)AlGaN sample at this Al flux and some defects are visible at the top of the layer.

The improvement in material quality from ISAE growth is further emphasized when comparing (In)AlGaN and AlGaN films which were provided identical aluminum fluxes (Figure 2(b) and Figure 2(c)). These samples have markedly different growth rates and degrees of homogeneity, despite identical aluminum fluxes. Atom force microscopy (AFM) measurements (see Supplementary Materials) further highlight these differences. The (In)Al<sub>0.30</sub>Ga<sub>0.70</sub>N sample has a smooth surface, with a RMS roughness of ~0.5 nm over a 10x10 µm² area. The AlGaN sample with similar aluminum flux, however, had an RMS of ~7 nm over the same area. Note that this is most likely due to the considerably higher aluminum metal fraction of the AlGaN sample, which caused significant relaxation and thus a 3D growth mode. This film appears to have a reduced density of defects near the top of the layer, which may indicate that strain-related effects also contribute to the formation of Al-rich defects.

To further study the structure of m-plane (In)Al<sub>0.30</sub>Ga<sub>0.70</sub>N, a 30-repeat MQW was grown consisting of 5.5 nm (In)Al<sub>0.30</sub>Ga<sub>0.70</sub>N barriers and 2.9 nm In<sub>0.16</sub>Ga<sub>0.84</sub>N wells. Figure 3 shows HR-STEM images of this MQW, revealing the presence of mostly planar high-Al regions similar to those seen in the bulk layer (Figure 2(b)). We consider these defects to be representative of the growth conditions, and the small differences between Figure 2(b) and Figure 3 to be qualitatively

insignificant. In this MQW, the high-Al defects consist of few monolayer thick islands, typically less than 50 nm wide, and are relatively isolated from each other. Each of these defects appears directly below a region where the (In)AlGaN layer is thinner, resulting in a depressed heterointerface compared to the rest of the layer (Figure 3(a)). These features are emphasized in Figure 3(b). The thinning of the (In)AlGaN layer above these high-Al containing defects suggests a causal relationship between the formation of Al-rich regions and the reduced growth rate seen in m-plane AlGaN layers.

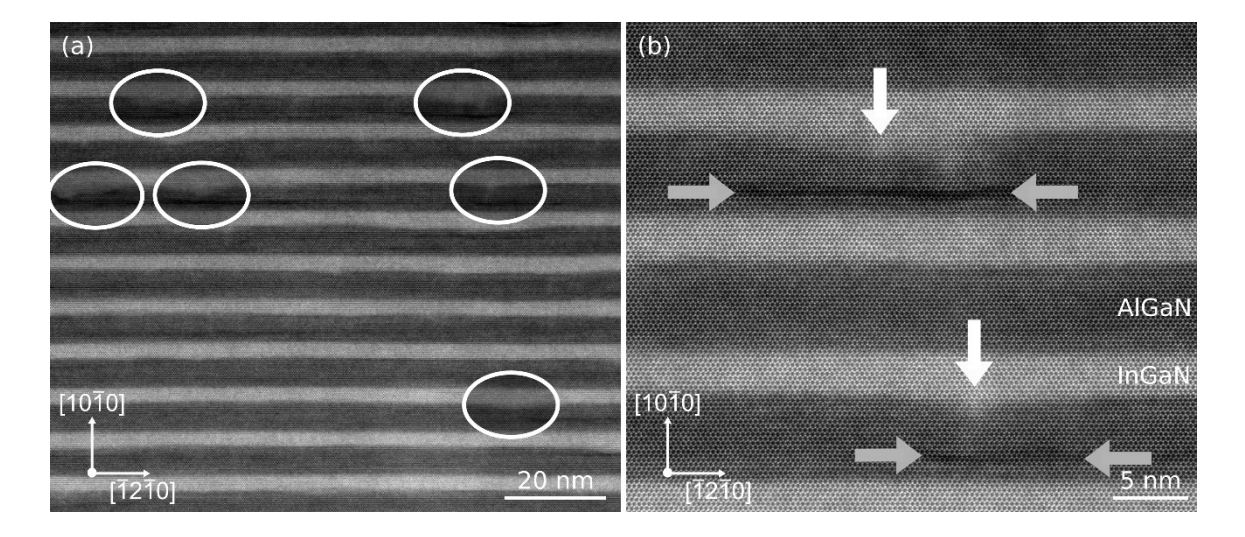


**Figure 3.** HR-STEM images of a 30 repeat (In)Al<sub>0.30</sub>Ga<sub>0.70</sub>N/In<sub>0.16</sub>Ga<sub>0.84</sub>N MQW structure. Lighter and darker regions represent the InGaN and AlGaN layers, respectively. High aluminum containing defects are visible in (a) and are outlined in white circles for clarity. Each of these defects appear below areas where the InGaN QW is thicker and protrudes down into the previous AlGaN layer. This is highlighted in (b), where grey arrows indicate the high-aluminum defect, and white arrows show the thicker area of the InGaN QW. The growth direction is along (1010).

This study is the first, to our knowledge, to report growth rate suppression across a wide range of aluminum fluxes for m-plane AlGaN, and to demonstrate the ability of ISAE to mitigate this

effect. We also found a compelling link between the formation of Al-rich regions and the reduction in growth rate. However, growth rate reduction with increasing metal flux has been observed in high-composition PAMBE m-plane AlGaN, as well as with different growth techniques and surface orientations. 19,21-24 Shirazi et al. observed a reduction in growth rate in high composition m-plane  $Al_vGa_{1-v}N$  (y > 0.50) grown by PAMBE at high-temperature.<sup>19</sup> They attributed the reduction in AlGaN growth rate to either the formation of an aluminum layer at the growth front which blocks gallium incorporation, or to the replacement of Ga-N dimers with Al-N dimers at c-edges. A similar effect was observed on [0001]-oriented sapphire substrates with metal-organic chemical vapor deposition (MOCVD). 21,22,24 These papers reported either a decrease in AlGaN growth rate with increasing trimethylaluminum (TMAI) flow rate or excessive aluminum incorporation. The phenomena were attributed to a suggested site-blocking effect by aluminum similar to that observed for NH<sub>3</sub> in MOCVD grown GaN<sup>25</sup> or nitrogen in NH<sub>3</sub> molecular-beam epitaxy (MBE).<sup>26</sup> Also noteworthy, a decrease in growth rate with increasing metal flux was also reported for lowtemperature InGaN layers grown by MBE on Si [111] substrates by Azadmand et al.<sup>23</sup> They attributed this phenomenon to the formation of metal droplets on the surface, which act as sinks for metal adatoms.

Further experimental and theoretical work needs to be done to determine the driving mechanism which leads to the observed reduction in the metal-rich growth rate. However, the observations in this work give us an increased understanding of the nature of this phenomenon. For our largest aluminum flux sample, the amount of nitrogen flux that must be lost to result in the observed decreased growth rate, approximately 3.08x10<sup>14</sup> atoms/cm<sup>2</sup>s, exceeds that of the provided aluminum flux (~1.72x10<sup>14</sup> atoms/cm<sup>2</sup>s) (Figure 1(a)). This suggests that Al-N dimers replacing incorporated Ga-N dimers from the surface cannot fully explain the phenomenon. If every Al-N dimer provided replaced a Ga-N dimer in the lattice, the resulting loss would not be sufficient to explain the reduction in growth rate. Effects from strain in the solid phase cannot fully explain the process either, as the strain states of the (In)Al<sub>0.30</sub>Ga<sub>0.70</sub>N and Al<sub>0.29</sub>Ga<sub>0.71</sub>N layers

should be similar, but we observe a significant difference in the nitrogen-limited growth rates and degree of homogeneity between these two layers (Figure 2(a) and Figure 2(b)).

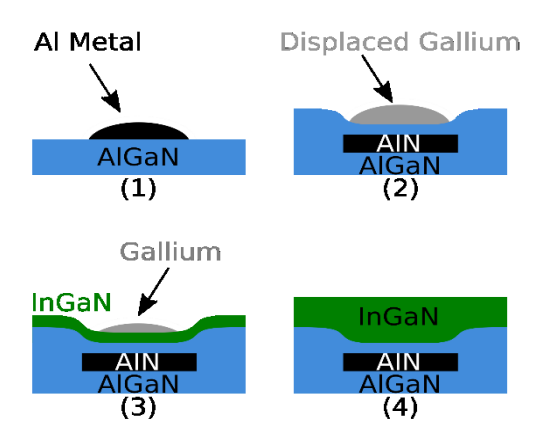


**Figure 4.** Aluminum metal clusters on the surface, exhibiting a site-blocking effect which prevents the incorporation of gallium (1). This results in a reduced AlGaN growth rate, leading to a thinner AlGaN layer and excess gallium on the surface (2). During the growth of the InGaN layer, this gallium is incorporated, leading to a locally thicker InGaN layer (3-4).

HR-STEM (Figure 2) combined with the measured average growth rates and aluminum compositions (Figure 1) suggest that the generation of high-aluminum containing defects is correlated to the reduction in growth rate observed in m-plane AlGaN layers. In fact, the direct spatial relationship between these phenomena, illustrated in Figure 3, suggests that the formation of these planar high-aluminum containing defects is directly responsible for the reduced growth rate of AlGaN layers. Therefore, we propose a model in which aluminum adatoms segregate at the growth front, and upon incorporation into the lattice, result in the Al-rich regions seen in Figure 2 and Figure 3. The segregation of these adatoms at the growth front may be due to the relatively strong Al-Al bond<sup>27</sup> coupled with high diffusion barriers on the m-plane surface compared to those on c-plane.<sup>28,29</sup> These Al-rich regions may exhibit a site-blocking effect, similar to that theoretically described by Goldstein and Ehrlich,<sup>30</sup> that suppresses the incorporation of gallium into the crystal, effectively reducing the net alloy growth rate. In bulk structures, this displaced gallium leads to

droplet formation on the surface. In AlGaN/InGaN MQWs, the displaced gallium is incorporated into the InGaN layer. Figure 4 illustrates how this model may result in the features seen in Figure 3. We speculate that an indium surfactant increases the diffusion length of aluminum adatoms, preventing clustering on the surface. This reduces the density of Al-rich regions on the growth front, and therefore in the material. Since Goldstein and Ehrlich suggest that groups of adatoms will have a site-blocking effect larger than random atomic distributions, with less aluminum clustering, the site-blocking effect will be reduced, allowing gallium to incorporate into the lattice and recovering the expected nitrogen-limited growth rate.

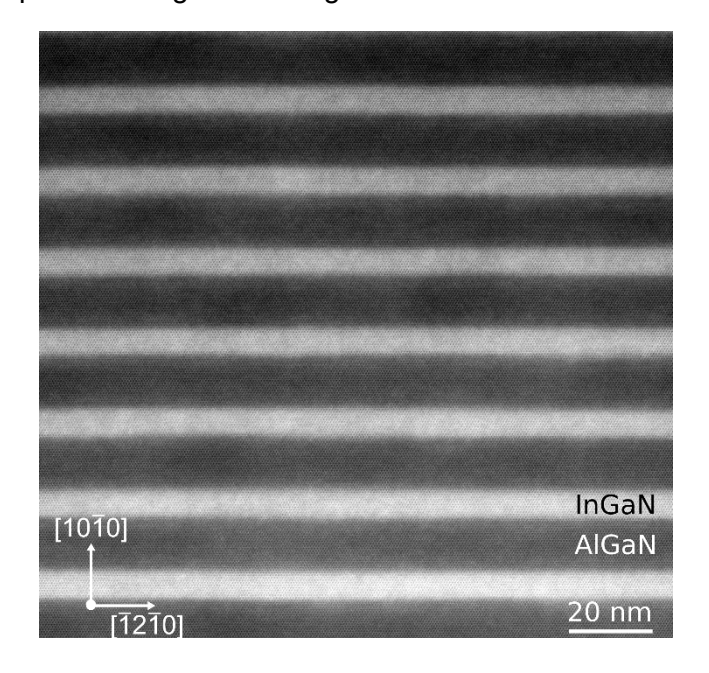


**Figure 5.** HR-STEM images of a 15 repeat (In)Al<sub>0.24</sub>Ga<sub>0.76</sub>N/In<sub>0.16</sub>Ga<sub>0.84</sub>N MQW structure with 3.4 nm wells and 5.8 nm barriers. Lighter and darker regions represent the InGaN and AlGaN layers, respectively. No high-Al containing defects are visible in the barriers. The growth direction is along  $(10\overline{1}0)$ .

Control of alloy composition is essential for the use of m-plane (In)AlGaN layers in electronic and optoelectronic devices. Previously, we reported that indium incorporation may be unavoidable in low-temperature, m-plane (In)AlGaN.<sup>12</sup> This was due to the observation that a gallium-rich

structure with an indium surfactant exhibited a non-negligible level of indium incorporation. However, we have shown here that the incorporated nitrogen increases when an indium surfactant is utilized in AlGaN samples with identical aluminum fluxes. Thus, it is necessary to use a higher gallium flux in an ISAE layer compared to that of a gallium-rich layer to maintain nitrogen-limited conditions and prevent indium incorporation. This methodology facilitates the growth of low-temperature, m-plane (In)AlGaN layers with little to no indium incorporation that is necessary for the development of (In)AlGaN/InGaN MQW structures with CBOs large enough to allow NIR ISB optical transitions. Figure 5 shows HR-STEM of a 15-repeat strain-balanced mplane (In)Al<sub>0.24</sub>Ga<sub>0.76</sub>N/In<sub>0.16</sub>Ga<sub>0.84</sub>N MQW structure grown by ISAE with little to no indium incorporation in the barrier. We note that the Ga flux was increased while the Al flux was decreased relative to the structure shown in Figure 3. No high-aluminum containing defects were visible in HR-STEM images of this structure. This is most likely due to the reduced aluminum molar fraction compared to the (In)Al<sub>0.30</sub>Ga<sub>0.70</sub>N/In<sub>0.16</sub>Ga<sub>0.84</sub>N structure presented in Figure 3. Band structures calculated using the nextnano3 software<sup>31</sup> predict a 597 meV CBO, which is sufficient to enable NIR ISB transitions. To our knowledge, this is the first demonstration of an m-plane AlGaN/InGaN structure with a large enough CBO to enable near-IR ISB transitions.

## 4. Conclusion

Bulk m-plane AlGaN films were grown on  $(10\overline{10})$ -oriented free-standing GaN substrates by PAMBE across a range of aluminum fluxes using either gallium-rich conditions or an indium surfactant. The growth rate of gallium-rich samples was found to exhibit an anomalous decrease with increasing aluminum flux. As a result, the average aluminum composition of these films increases super-linearly with increasing aluminum flux. ISAE layers, in contrast, did not show a significant variation in growth rate with aluminum flux. The aluminum composition of ISAE films

increased linearly with the aluminum flux, as expected. Moreover, the ISAE layers exhibited a reduced density of high-Al containing defects and negligible indium incorporation.

Spatial correlation of high-Al containing defects with areas of locally thinner AlGaN layers observed in a MQW structure suggests that the reduced growth rate is a consequence of the aluminum-rich defects. This phenomenon is tentatively explained by aluminum adatoms clustering on the surface and exhibiting a site-blocking effect that prevents the incorporation of gallium. As a result, the local AlGaN growth rate is reduced and the local aluminum composition is increased. We propose that ISAE mitigates this phenomenon by increasing surface diffusion, which reduces clustering and therefore the site-blocking effect. We used these results to grow a high-quality strain-balanced (In)Al<sub>0.24</sub>Ga<sub>0.76</sub>N/In<sub>0.16</sub>Ga<sub>0.84</sub>N MQW structure that has potential applications for NIR optoelectronic applications.

# **Supplementary Material**

See supplementary material for AFM and optical microscopy images of the samples discussed in this paper.

## **Acknowledgements**

We acknowledge support from the National Science Foundation (NSF). B.D. was supported by the NSF award no. ECCS-1607173. T.N., Y.C., and O.M. acknowledge partial support from NSF awards DMR-1610893 and DMR-2004462. All STEM imaging and analyses were performed at the Electron Microscopy Facility at the Birck Nanotechnology Center, Purdue University.

## **Data Availability**

The data that supports the findings of this study are available within the article.

### References

<sup>1</sup> O. Ambacher, J. Phys. D: Appl. Phys. **31**, 2653 (1998).

- <sup>2</sup> J. Wu, W. Walukiewicz, W. Shan, K.M. Yu, J.W. Ager, S.X. Li, E.E. Haller, H. Lu, and W.J. Schaff, Journal of Applied Physics **94**, 4457 (2003).
- <sup>3</sup> S.C. Jain, M. Willander, J. Narayan, and R.V. Overstraeten, Journal of Applied Physics **87**, 965 (2000).
- <sup>4</sup> F. Wu, W. Tian, W.Y. Yan, J. Zhang, S.C. Sun, J.N. Dai, Y.Y. Fang, Z.H. Wu, and C.Q. Chen, Journal of Applied Physics **113**, 154505 (2013).
- <sup>5</sup> M. Beeler, C. Bougerol, E. Bellet-Amalric, and E. Monroy, Appl. Phys. Lett. **103**, 091108 (2013).
- <sup>6</sup> T. Langer, H. Jönen, A. Kruse, H. Bremers, U. Rossow, and A. Hangleiter, Appl. Phys. Lett. **103**, 022108 (2013).
- <sup>7</sup> M.N. Fireman, B. Bonef, E.C. Young, N. Nookala, M.A. Belkin, and J.S. Speck, Journal of Applied Physics **122**, 075105 (2017).
- <sup>8</sup> E. Kuokstis, C.Q. Chen, M.E. Gaevski, W.H. Sun, J.W. Yang, G. Simin, M. Asif Khan, H.P. Maruska, D.W. Hill, M.C. Chou, J.J. Gallagher, and B. Chai, Applied Physics Letters **81**, 4130 (2002).
- <sup>9</sup> P. Waltereit, O. Brandt, A. Trampert, H.T. Grahn, J. Menniger, M. Ramsteiner, M. Reiche, and K.H. Ploog, Nature **406**, 865 (2000).
- <sup>10</sup> J.S. Speck and S.F. Chichibu, MRS Bull. **34**, 304 (2009).
- <sup>11</sup> A. Senichev, B. Dzuba, T. Nguyen, Y. Cao, M.A. Capano, M.J. Manfra, and O. Malis, APL Materials **7**, 121109 (2019).
- <sup>12</sup> B. Dzuba, A. Senichev, T. Nguyen, Y. Cao, R.E. Diaz, M.J. Manfra, and O. Malis, Journal of Applied Physics **128**, 115701 (2020).
- <sup>13</sup> T.M. Al tahtamouni, A. Sedhain, J.Y. Lin, and H.X. Jiang, Appl. Phys. Lett. **92**, 092105 (2008).
- <sup>14</sup> Z. Liang, X. Zhang, Q. Dai, H. Luan, J. Zhao, Z. Wu, G. Hu, and Y. Cui, J Mater Sci: Mater Electron **28**, 15217 (2017).

- <sup>15</sup> Q. Dai, X. Zhang, Z. Liang, G. Yang, Z. Wu, S. Chen, J. Zhao, C. Meng, J. Wang, and Y. Cui, Opt. Mater. Express, OME **8**, 24 (2018).
- <sup>16</sup> E. Monroy, B. Daudin, E. Bellet-Amalric, N. Gogneau, D. Jalabert, F. Enjalbert, J. Brault, J. Barjon, and L.S. Dang, Journal of Applied Physics **93**, 1550 (2003).
- <sup>17</sup> P. Pramanik, S. Sen, C. Singha, A.S. Roy, A. Das, S. Sen, A. Bhattacharyya, D. Kumar, and D.V. Sridhara Rao, Journal of Crystal Growth **439**, 60 (2016).
- <sup>18</sup> J. Neugebauer, T.K. Zywietz, M. Scheffler, J.E. Northrup, H. Chen, and R.M. Feenstra, Physical Review Letters **90**, (2003).
- <sup>19</sup> M. Shirazi-HD, R.E. Diaz, T. Nguyen, J. Jian, G.C. Gardner, H. Wang, M.J. Manfra, and O. Malis, Journal of Applied Physics **123**, 161581 (2018).
- <sup>20</sup> J.R. Jenny, J.E. Van Nostrand, and R. Kaspi, Appl. Phys. Lett. **72**, 85 (1998).
- <sup>21</sup> J. Han, J.J. Figiel, M.H. Crawford, M.A. Banas, M.E. Bartram, R.M. Biefeld, Y.K. Song, and A.V. Nurmikko, Journal of Crystal Growth **195**, 291 (1998).
- <sup>22</sup> D.G. Zhao, Z.S. Liu, J.J. Zhu, S.M. Zhang, D.S. Jiang, H. Yang, J.W. Liang, X.Y. Li, and H.M. Gong, Applied Surface Science **253**, 2452 (2006).
- <sup>23</sup> M. Azadmand, L. Barabani, S. Bietti, D. Chrastina, E. Bonera, M. Acciarri, A. Fedorov, S. Tsukamoto, R. Nötzel, and S. Sanguinetti, Sci Rep **8**, 11278 (2018).
- <sup>24</sup> S. Kim, J. Seo, K. Lee, H. Lee, K. Park, Y. Kim, and C.S. Kim, J. Cryst. Growth **245**, 247 (2002).
- <sup>25</sup> O. Briot, J.P. Alexis, B. Gil, and R.L. Aulombard, MRS Online Proceedings Library (OPL) **395**, (1995).
- <sup>26</sup> N. Grandjean, J. Massies, F. Semond, S.Yu. Karpov, and R.A. Talalaev, Appl. Phys. Lett. **74**, 1854 (1999).
- <sup>27</sup> Y.-R. Luo, *Comprehensive Handbook of Chemical Bond Energies* (CRC Press, Boca Raton, 2007).
- <sup>28</sup> V. Jindal and F. Shahedipour-Sandvik, Journal of Applied Physics **105**, 084902 (2009).

- <sup>29</sup> L. Lymperakis and J. Neugebauer, Phys. Rev. B **79**, 241308 (2009).
- <sup>30</sup> J.T. Goldstein and G. Ehrlich, Surface Science **420**, 1 (1999).
- <sup>31</sup> S. Birner, T. Zibold, T. Andlauer, T. Kubis, M. Sabathil, A. Trellakis, and P. Vogl, IEEE Transactions on Electron Devices **54**, 2137 (2007).